IOP Publishing Journal of Physics B: Atomic, Molecular and Optical Physics
J. Phys. B: At. Mol. Opt. Phys. **53** (2020) 064002 (13pp) https://doi.org/10.1088/1361-6455/ab5bac

Asymmetry of molecular frame photoelectron angular distributions in H_2^+ by intense two-color attosecond pulses: coherent excitation and charge migration effects

Kai-Jun Yuan[1,2,3] **and André D Bandrauk**[2]

[1] Institute of Atomic and Molecular Physics, Jilin University, Changchun, 130012, People's Republic of China
[2] Laboratoire de Chimie Théorique, Faculté des Sciences, Université de Sherbrooke, Sherbrooke, Québec J1K 2R1, Canada

E-mail: kjyuan@jlu.edu.cn and andre.bandrauk@usherbrooke.ca

Received 11 November 2019
Accepted for publication 26 November 2019
Published 14 February 2020

Abstract

Molecular frame photoelectron angular distributions (MFPADs) are theoretically studied by intense two-color attosecond linearly polarized laser pulses. Simulations are performed on aligned H_2^+ from numerical solutions of corresponding time-dependent Schrödinger equations. Asymmetric MFPADs are produced by a time-delayed soft x-ray attosecond pulse in the presence of an extreme ultraviolet (XUV) pump pulse. We present the dependence of the asymmetry ratio Γ of the MFPADs on the laser parameters of the pump-probe pulses. The asymmetry ratio Γ varies with the time delay, illustrating the coherent superposition of electronic states. Altering the phase, intensity and duration of the pump pulse gives rise to a modulation of the asymmetry ratio Γ as well. Moreover, the asymmetry of the MFPADs disappears in the case of long duration probe pulses, illustrating the coherent charge migration dynamics on the attosecond time scale.

Keywords: charge migration, photoelectron diffraction, pump probe spectroscopy, asymmetry

(Some figures may appear in colour only in the online journal)

1. Introduction

Following rapid developments of ultrafast laser technology, visualization and manipulation of electron motion in atomic and molecular systems on its natural time scale, the attosecond (1 as $= 10^{-18}$ s), has attracted great interest in the field of ultrafast science [1–5]. Recently, the shortest attosecond pulse with a duration of 43 as pulse has been produced [6]. Time-resolved photoelectron spectroscopy based pump-probe techniques has been widely used as an efficient tool for investigations of electron and nuclear dynamics in molecular systems [7–13]. A coherent transition between ground and excited states of targets is initiated by an ultrashort pump laser pulse, and subsequently its evolution with time is monitored by a time delayed probe pulse. Electrons have a great potential for probing the time-resolved transient structure of matter via ultrashort photoelectron spectroscopy. One can now envisage the emergence of laser-induced electron interference and diffraction as efficient methods for orbital imaging [14–22]. In long wavelength tunnelling photoionization processes, the interference between different electron trajectories originating within the same or different cycles gives rise to various interferometric structures, which have recently been observed in photoelectron momentum spectra by a time-resolved photoelectron holography technique [23, 24]. Recently, laser-induced electron diffraction has been used to

[3] Author to whom any correspondence should be addressed.

image Renner–Teller nonadiabatic vibronic dynamics in neutral molecular systems within picometer and attosecond resolutions [25].

Interference asymmetry of photoionization accessed coherently through multiple excitation pathways has acquired increasing relevance for photophysics and photochemistry triggered by bichromatic laser pulses. It has been shown that angular distributions of excitation and dissociation products in molecules can be controlled directly by varying pulse relative phases, e.g. in [26, 27, 28]. Measuring photoelectron angular and energy distributions has been used to monitor electron dynamics in coherent electron wave packets (CEWPs), thus revealing the effects of multi-pathway quantum interference [29, 30]. It has also been found that with high-frequency UV light, the asymmetry in angular distributions of molecular above-threshold ionization, due to multiple ionization pathway interference, is critically sensitive to the pulse carrier envelope phase (CEP), the time delay between pulses, and photoelectron kinetic energies [31]. The influence of photon energies and CEPs in atomic resonant ionization processes has also been presented [32]. Under resonant excitation, the interference asymmetry is also shown to be sensitive to pulse intensities [33]. Interference effects among ion rotational channels during photoionization have been exploited to control the asymmetry of photoelectron angular distributions at specific photoelectron energies [34]. In addition, interference effects of electronic states on vibrationally resolved photoionization in molecules have been studied [35, 36]. Two time-delayed, circularly polarized attosecond UV pulses of the same frequency produce spiral electron vortices in atomic photoionization momentum distributions [37, 38, 39, 40, 41]. It is found that the vortex patterns can only be observed for two oppositely handed, i.e., counter-rotating, circularly polarized fields and are absent for the same helicity (co-rotating pulses). However, by using bichromatic circularly polarized pulses, such a spiral structure can be produced in molecular frame photoelectron momentum distributions (MFPMDs) for both co-rotating and counter-rotation cases [42–44]. Time-resolved asymmetric photoelectron distributions have recently been used to explore electron coherence in molecular resonant excitation processes [45, 46]. Analytical and numerical study of the attosecond x-ray photoionization of a coherent superposition of molecular electronic states shows that asymmetric photoelectron momentum distributions measure the momentum asymmetry of initial wave packets due to molecular interference, and thus are related to the direction of charge migration [47].

The process of ultrafast coherent excitation is a fundamental and important phenomenon in photon-induced molecular reactions [48–65]. It arises from coherent population excitation in multiple electronic states, thus offering an approach to imaging molecular orbitals and monitoring electron motion. Recently, studies showed that quantum control of electron flux during intramolecular charge migration can be produced by designing an ultrafast laser pulse that prepares the system in a selective electronic state [66–68]. It has been also found that electron currents are sensitive to the polarization and helicity of the driving pulse, i.e., the

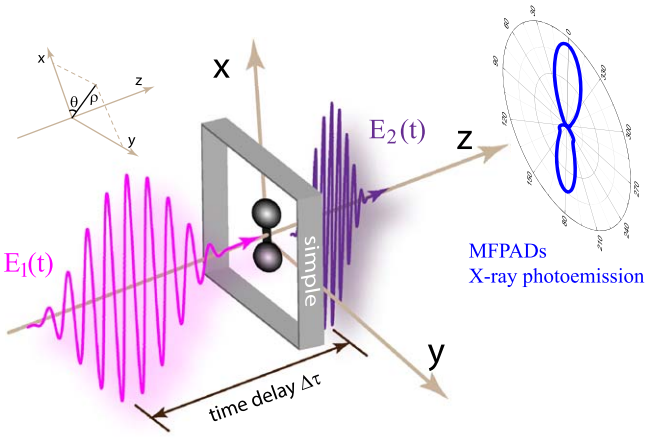

Figure 1. Illustration of photoionization processes in the aligned molecular ion H_2^+ by time-delay two-color laser pulses. The pump pulse $E_1(t)$ induces a resonant $\sigma_g - \sigma_u/\pi_u$ excitation. Subsequently, a soft x-ray attosecond probe pulse $E_2(t)$ is used to ionize the excited molecule, producing asymmetric MFPADs. $\Delta\tau$ is the time-delay between the two pulses. The molecule H_2^+ is aligned along the molecular x axis, and the pump and probe pulses with their field vectors along the x axis propagate along the z axis.

symmetry of the excited electronic state [69]. Imaging of charge migration dynamics is a challenge in real time in ultrafast spectroscopy due to its high spatio–temporal resolutions. Attosecond charge migration has been, for the first time, measured in experiments by linearly polarized high-order harmonic generation in ionized iodoacetylene via attosecond electron recollision [70]. Angular electronic fluxes can also be used to reconstruct electron charge migration in excited benzene by preparing a coherent electronic state [67, 69], which can be monitored in photoelectron momentum spectra by time-delayed high frequency attosecond pulses [45]. Molecular photoelectron diffraction patterns, which encode information of the symmetry of molecular orbitals and molecular bondings, have been used to monitor electron coherence and charge migration by pump-probe pulses [71–73]. Moreover, photoelectron holography has also been proposed to monitor coherent electron excitation [74, 75].

In the present work, we present the asymmetry of MFPADs in ultrafast molecular photoionization processes by intense two-color attosecond laser pulses, as illustrated in figure 1. The molecular ion H_2^+ is used as a benchmark model which can be fully investigated to describe the electron dynamics [76] and is aligned [77]. An XUV pump pulse is employed to excite the molecule, leading to a resonant excitation between two electronic states, the ground $1s\sigma_g$ and excited $2p\sigma_u$ states. Subsequently, a time-delayed soft x-ray attosecond probe pulse is used to ionize the excited molecule. Results show that the asymmetric MFPADs of the x-ray photoemission are dependent on the parameters of the pump-probe pulses. The asymmetric distributions of x-ray photoemission yields result from the coherent electron which evolves periodically in molecules, thus allowing the monitoring of molecular charge migration. Simulation results are obtained by numerically solving the corresponding time-dependent Schrödinger equation (TDSE). The molecular

rotational and vibrational motions on picosecond (1 ps = 10^{-12} s) and femtosecond (1fs = 10^{-15} s) time scales are ignored because these effects are much slower than the laser–molecule interaction that occurs within the attosecond time scale.

The paper is organized as follows. We briefly describe the computational method for solving TDSEs of the aligned molecular ion H_2^+ in section 2. Results of asymmetric photoelectron distributions produced by pump and probe techniques are presented and discussed in section 3. We describe time dependent ultrafast photoionization models to understand these ultrafast phenomena. Finally, in section 4 we summarize our findings. Throughout this paper, atomic units (au) are used unless otherwise stated.

2. Numerical and computational methods

For an aligned single electron molecular ion H_2^+ interacting with linearly polarized laser fields $\mathbf{E}(t)$, the corresponding three-dimensional (3D) TDSE within Born–Oppenheimer approximation and static nuclear frames reads as,

$$i\frac{\partial}{\partial t}\psi(\mathbf{r}, t) = [T(\mathbf{r}) + V_{en}(\mathbf{r}) + V_L(\mathbf{r}, t)]\psi(\mathbf{r}, t). \quad (1)$$

$T(\mathbf{r})$ and $V_{en}(\mathbf{r})$ are the kinetic energy operators of the electron and the electron–nucleus Coulombic attraction. We adopt cylindrical coordinates $\mathbf{r} = (\rho, \theta, z)$ with $x = \rho\cos\theta$, $y = \rho\sin\theta$ to describe the ultrafast electron dynamics. The molecule is aligned along the x axis at equilibrium. Then, the kinetic (Laplacian) operator gives

$$T(\rho, \theta, z) = -\frac{1}{2\rho}\frac{\partial}{\partial\rho}\left(\rho\frac{\partial}{\partial\rho}\right) - \frac{1}{2\rho^2}\frac{\partial^2}{\partial\theta^2} - \frac{1}{2}\frac{\partial^2}{\partial z^2}, \quad (2)$$

and the electron–nuclear potential

$$V_{en}(\rho, \theta, z) = -\frac{1}{\sqrt{\rho^2 + R\rho\cos\theta + R^2/4 + z^2 + \alpha}} - \frac{1}{\sqrt{\rho^2 - R\rho\cos\theta + R^2/4 + z^2 + \alpha}}, \quad (3)$$

$R = 2$ au is the equilibrium molecular internuclear distance and $\alpha = 0.35$ is a soft parameter which is used to remove the singularity in the Coulomb potential in equation (3), allowing the accurate production of the electronic state potential energies of H_2^+ [78]. As illustrated in figure 1, the molecule is aligned along the x axis. The two laser pulses are linearly polarized along the x or y axis, propagate along the z axis and perpendicular to the molecular (x, y) plane. The radiative interaction between the laser field and the electron $V_L(\mathbf{r}) = \mathbf{r}\cdot\mathbf{E}(t)$ is described in the length gauge. The total fields $\boldsymbol{E}(\mathrm{t}) = \mathbf{E}_1(t) + \mathbf{E}_2(t)$ have the forms

$$\mathbf{E}_1(t) = \hat{e}_{x/y}E_1 f(t)\cos(\omega_1 t + \phi_1), \quad (4)$$

and

$$\mathbf{E}_2(t - \Delta\tau) = \hat{e}_{x/y}E_2 f(t - \Delta\tau)\cos[\omega_2(t - \Delta\tau) + \phi_2), \quad (5)$$

where $\Delta\tau$ is the time delay between the two pulses with CEPs ϕ_1 and ϕ_2 and $\hat{e}_{x/y}$ is the laser polarization direction. A smooth pulse envelope $f_{1/2} = \sin^2(\pi t/T_{1/2})$ for maximum amplitude $E_{1/2}$, corresponding to intensity $I_{1/2} = c\varepsilon_0 E_{1/2}^2/2$ and duration $T_{1/2} = 10\tau_{1/2}$ are used, where one optical cycle period $\tau_{1/2} = 2\pi/\omega_{1/2}$. This pulse satisfies the total zero area $\int E_{1/2}(t)dt = 0$ in order to exclude static field effects [1]. Time durations T_2 are chosen to be $\sim 100 - 200$ as, time much faster than the H_2^+ vibrational period $\tau_v \sim 10$ fs, so that charge migration due to electron motion is the main dynamics in the presence of static nuclei.

The 3D TDSE in equation (1) for the aligned molecule H_2^+ is numerically solved by a second order split operator method, which conserves unitarity in the time step δt combined with a fifth order finite difference method and Fourier transform technique in the spatial steps $\delta\rho$, δz, and $\delta\theta$ [79, 80]. The time step is taken to be $\delta t = 0.01$ au $= 0.24$ as. The spatial discretization is $\delta\rho = \delta z = 0.25$ au for a radial grid range $0 \leqslant \rho \leqslant 128$ au (6.77 nm) and $|z| \leqslant 32$ au (1.69 nm), and the angle grid size $\delta\theta = 0.025$ radian. To prevent unphysical effects due to the reflection of the wave packet from the boundary, we multiply $\psi(\rho, \theta, z, t)$ by a 'mask function' or absorber in the radial coordinates ρ with the form $\cos^{1/8}[\pi(\rho - \rho_a)/2\rho_{abs}]$. For all the results reported here we set the absorber domain at $\rho_a = \rho_{max} - \rho_{abs} = 104$ au with $\rho_{abs} = 24$ au, exceeding well the field-induced electron oscillation $\alpha_d = E_{1/2}/\omega_{1/2}^2$ of the electron.

Photoionization yields, i.e., MFPADs, are calculated by a Fourier transform of the 3D time-dependent electronic wavefunction $\psi(\rho, \theta, z, t)$ which exactly describes the electron dynamics in the continuum [81]:

$$\mathcal{J}_l(\theta, z, E)|_{\rho_f} = \int_{t_p}^{\infty} \psi(\theta, z, t)|_{\rho_f}\, e^{iEt}dt,$$
$$\mathcal{J}_r(\theta, z, E)|_{\rho_f} = \int_{t_p}^{\infty} \frac{\partial\psi(\theta, z, t)}{\partial\rho}|_{\rho_f}\, e^{iEt}dt,$$
$$\mathcal{J}(\theta, E) \sim \mathrm{Re}\left[\frac{1}{2i}\int J_l^*(\theta, z, E)|_{\rho_f} J_r(\theta, z, E)|_{\rho_f} dz\right], \quad (6)$$

where t_p is the time after the pulse turn off and $\rho_f = 100$ au is an asymptotic point before the wavepacket is absorbed. $E_e = p^2/2$ is the kinetic energy of an ionized electron with wave vector $k = p = 2\pi/\lambda_e$, and $p = (p_x^2 + p_y^2)^{1/2}$ is the momentum of a photoelectron of wavelength λ_e. Since the ionization occurs in the laser polarization (x, y) molecular plane, we define θ as the angle between the electron momentum $\mathbf{p}$ and the x polarization axis. With the transformation $p_x = p\cos\theta$ and $p_y = p\sin\theta$, we then obtain the two-dimensional (2D) momentum distributions of photoelectrons from equation (6). MFPADs at photoelectron kinetic energy E_e are obtained by integrating over the one-photon energy, where the spectra width of the probe pulse $\Delta\omega \approx \omega_2/3$,

$$\mathcal{J}^{E_e}(\theta) = \int_{E_e - \omega_2/3}^{E_e + \omega_2/3} dE\mathcal{J}(\theta, E), \quad (7)$$

corresponding to the main one-photon ω_2 frequency of absorption.

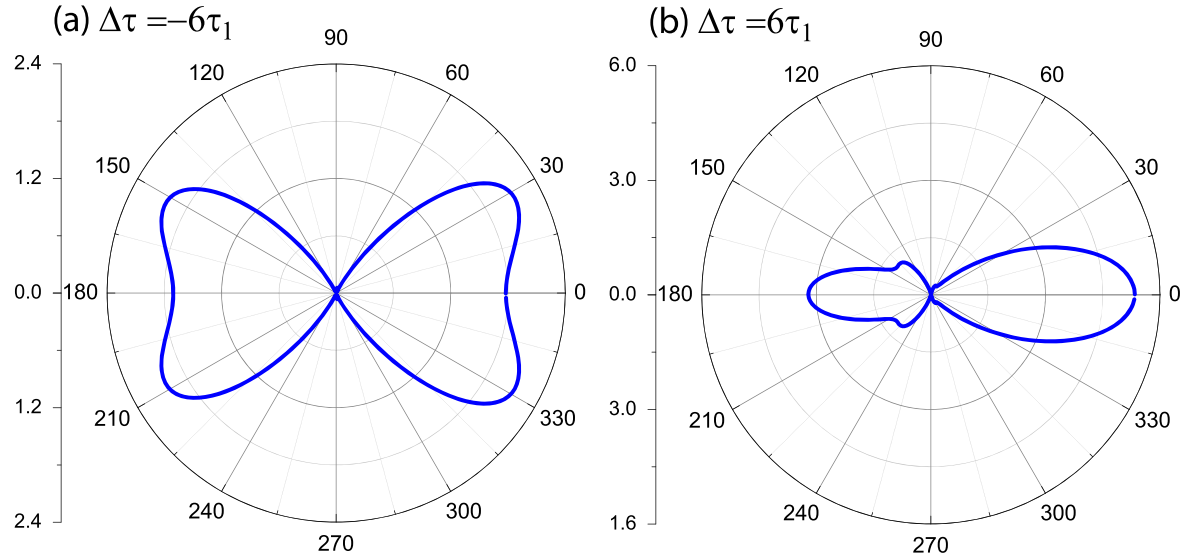

Figure 2. MFPADs of the molecular H_2^+ aligned along the x axis at $R = 2$ au by time-delayed two-color $\lambda_1 = 100$ nm and $\lambda_2 = 5$ nm laser pulses, with their field vectors polarized along the molecular R/x axis. The time delays are, respectively, chosen as (a) $\Delta\tau = -6\tau_1$ and (b) $6\tau_1$, i.e., the pulse $E_2(t)$ switches on before and after the pulse $E_1(t)$. The pulse intensities $I_{1/2} = 2.75 \times 10^{13}$ W/cm^2 ($E_{1/2} = 2.8 \times 10^{-2}$ au), durations $T_{1/2} = 10\tau_{1/2}$, i.e., $T_1 = 3.31$ fs (1.655 fs FWHM) and $T_2 = 165.4$ as (83 as FWHM), and phases $\phi_1 = \phi_2 = 0$ are used. Arbitrary units of MFPADs are used.

3. Results and discussions

Here we focus on the photoionization process in the molecule H_2^+ which is used as a benchmark system by intense two-color ultrashort laser pulses. Time-delayed pump and probe pulses are used to excite and ionize the molecule. The molecule H_2^+ is aligned along the x axis at equilibrium, and the pump and probe pulses with their field vectors along the x/y axis propagate along the z axis, as illustrated in figure 1. We measure the ultrafast x-ray MFPADs to explore the coherent electron dynamics in molecules. For these processes by high-frequency pulses, multi-photon ionization dominates with the Keldysh parameter $\gamma = \sqrt{I_p/2U_p} \gg 1$, where I_p is the molecular ionization potential and $U_p = E_{1/2}^2/4\omega_{1/2}^2$ denotes the ponderomotive energy [1]. Since U_p is very weak, the modification of the ionization potential by laser-induced Stark shifts can be ignored as well. Moreover, the dipole approximation, in which the spatial dependence and magnetic component of the external field are neglected, remains valid.

3.1. Asymmetry of MFPADs in time-delayed two-color laser fields

We first consider the dependence of the MFPADs on the time delay $\Delta\tau$ between the pump $\mathbf{E}_1(t)$ and probe $\mathbf{E}_2(t)$ pulses. Figure 2 displays the results of the MFPADs, $\mathcal{J}^{E_e}(\theta)$ calculated from equation (7), at two different time delays: (a) $\Delta\tau = -6\tau_1$ and (b) $6\tau_1$, i.e., the pulse $E_2(t)$ switches on before and after the pulse $E_1(t)$. The pulse wavelengths are respectively $\lambda_1 = 100$ nm ($\omega_1 = 0.45$ au) and $\lambda_2 = 5$ nm ($\omega_2 = 9.1$ au). The same pulse intensities and durations are used at $I_{1/2} = 2.75 \times 10^{13}$ W/cm^2 ($E_{1/2} = 2.8 \times 10^{-2}$ au), $T_{1/2} = 10\tau_{1/2}$, i.e., $T_1 = 3.31$ fs, corresponding to 1.655 fs full width at half maximum (FWHM) and $T_2 = 165.4$ as (83 as FWHM). The pulse phases are fixed at $\phi_1 = \phi_2 = 0$. Of note is that the vibrational period of H_2^+ $\tau_v \sim 10$ fs. The duration T_2 on the attosecond time scale is much faster than proton motion, so one observes charge migration from electron transfer between the protons.

In figure 2 it is found that the structure of the simulated MFPADs is sensitive to the time delay $\Delta\tau$. At $\Delta\tau = -6\tau_1$, symmetric distributions are obtained due to the symmetric initial σ_g orbit, where the MFPADs exhibit four angular nodes at angles $\pm 30°$ and $180° \pm 30°$. Altering the time delay leads to a variance of the photoelectron distributions due to creation of a superposition of the $1s\sigma_g$ and $2p\sigma_u$ states. At $\Delta\tau = 6\tau_1$ one finds that asymmetric MFPADs are produced. The photoionization yields are mainly localized in the right half plane, $90° \geqslant \theta \geqslant -90°$ (270°). The angular nodes are also suppressed and the photoelectron distributions lie along the molecular R/x axis. In the case of $\Delta\tau = -6\tau_1$, the probe pulse $E_2(t)$ switches on before the pump pulse $E_1(t)$. The x-ray photoelectron distribution mainly comes from the ground $1s\sigma_g$ electronic state. However, at $\Delta\tau = 6\tau_1$, the molecule is excited resonantly by the pump pulse, from which the soft x-ray pulse produces photoelectron yields. As a result, the coherent excitation modifies the time-delayed x-ray photoemission via attosecond time dependent electron charge migration.

The modulation of the MFPADs by the time delay $\Delta\tau$ illustrates the molecular coherent electron dynamics induced by the $\lambda_1 = 100$ nm pump pulse. A $\sigma_g - \sigma_u$ resonant excitation occurs from the electronic ground $1s\sigma_g$ state, $\psi_{\sigma_g}(\mathbf{r})$ with the eigenenergy E_{σ_g} to the electronic excited $2p\sigma_u$ state, $\psi_{\sigma_u}(\mathbf{r})$ with the eigenenergy E_{σ_u}. The energies for the $1s\sigma_g$ and $2p\sigma_u$ states are respectively $E_{\sigma_g} = -1.08$ au and $E_{\sigma_u} = -0.65$ au in the numerical simulations. Since $\omega_1 \cong \Delta E = E_{\sigma_u} - E_{\sigma_g} = 0.45$ au, a coherent superposition of the two

electronic states is therefore created due to a strong charge–resonance excitation [82]

$$\psi_c(\mathbf{r}, t) = c_{\sigma_g}(t)\psi_{\sigma_g}(\mathbf{r})e^{-iE_{\sigma_g}t} + c_{\sigma_u}(t)\psi_{\sigma_u}(\mathbf{r})e^{-iE_{\sigma_u}t}. \quad (8)$$

Here $c_{\sigma_g}(t)$ and $c_{\sigma_u}(t)$ are the occupation coefficients. The electron density distribution of the coherent superposition electronic state in equation (8) is then described by,

$$\begin{aligned}\mathcal{D}(\mathbf{r}, t) &= |\psi_c^{\pm}(\mathbf{r}, t)|^2 \\ &= |c_{\sigma_g}(t)\psi_{\sigma_g}(\mathbf{r})|^2 + |c_{\sigma_u}(t)\psi_{\sigma_u}(\mathbf{r})|^2 \\ &\quad + 2|c_{\sigma_g}(t)c_{\sigma_u}(t)|\psi_{\sigma_g}(\mathbf{r})\psi_{\sigma_u}(\mathbf{r})\cos(\Delta E t). \end{aligned} \quad (9)$$

The coherent electron dynamics are composed of two electronic state densities, $\mathcal{D}^{(g)}(\mathbf{r}) = |c_{\sigma_g}(t)\psi_{\sigma_g}(\rho, z)|^2$ and $\mathcal{D}^{(u)}(\mathbf{r}) = |c_{\sigma_u}(t)\psi_{\sigma_u}(\mathbf{r})|^2$, and their interfering superposition $\mathcal{D}^{(g,u)}(\mathbf{r}, t) = \mathcal{C}(\mathbf{r}, t)\cos(\Delta E t)$, where $\mathcal{C}(\mathbf{r}, t) = 2|c_{\sigma_g}(t)c_{\sigma_u}(t)|\psi_{\sigma_g}(\mathbf{r})\psi_{\sigma_u}(\mathbf{r})$. The oscillation period of the coherent electron wavepacket is $\tau^{co} = 2\pi/\Delta E = 331$ as $= \tau_1$.

The photoemission yields from the superposition state $\psi_c(\mathbf{r}, t)$ in equation (8) can be derived based on the ultrafast photoionization delta-function pulse model [14]. The instantaneous transition amplitude to a continuum state of momentum $\mathbf{p}$ can be given by

$$\mathcal{F}(\mathbf{p}, t) = \left| (2\pi)^{-3/2} \int d\mathbf{r} e^{-i\mathbf{p}\cdot\mathbf{r}} e^{-i\mathbf{E}\cdot\mathbf{r}} \psi_c(\mathbf{r}, t) \right|^2. \quad (10)$$

The wavefunctions $\psi_{\sigma_g}(\mathbf{r})$ and $\psi_{\sigma_u}(\mathbf{r})$ in equation (8) are respectively linear combinations of a hydrogenic 1s orbital localized at $\pm R/2$. Then the coherent state transition amplitude $\mathcal{F}(\mathbf{p}, t)$ in equation (1) is given by [14, 83]

$$\begin{aligned}\mathcal{F}(\mathbf{p}, t) \sim &|c_{\sigma_g}(t)\cos[(\mathbf{p} + \mathbf{E}) \cdot \mathbf{R}/2]\psi_{1s}(\mathbf{p} + \mathbf{E})|^2 \\ &+ |c_{\sigma_u}(t)\sin[(\mathbf{p} + \mathbf{E}) \cdot \mathbf{R}/2]\psi_{1s}(\mathbf{p} + \mathbf{E})|^2 \\ &+ |c_{\sigma_g}(t)c_{\sigma_u}(t)|\sin[(\mathbf{p} + \mathbf{E}) \cdot \mathbf{R}/2] \\ &\times \cos(\Delta E t)|\psi_{1s}(\mathbf{p} + \mathbf{E})|^2. \end{aligned} \quad (11)$$

In this work, the pulse field strength $\mathbf{E}$ can be ignored to describe high-frequency photoemission yields, since the used intensities induce negligible ponderomotive energies $U_p = 2E_{1/2}^2/4\omega_{1/2}^2 \ll I_p$ and $E \ll p$. The transition amplitude, i.e., the momentum distributions of the photoelectron in equation (2), can be simply expressed as

$$\begin{aligned}\mathcal{F}(p, \theta, t) &= \mathcal{F}^{(\sigma_g)}(p, \theta, t) + \mathcal{F}^{(\sigma_u)}(p, \theta, t) \\ &\quad + \mathcal{F}^{(\sigma_g,\sigma_u)}(p, \theta, t) \\ &\sim |c_{\sigma_g}(t)\cos(pR\cos\theta/2)\psi_{1s}(p)|^2 \\ &\quad + |c_{\sigma_u}(t)\sin(pR\cos\theta/2)\psi_{1s}(p)|^2 \\ &\quad + |c_{\sigma_g}(t)c_{\sigma_u}(t)|\sin(pR\cos\theta/2) \\ &\quad \times \cos(\Delta E t)|\psi_{1s}(p)|^2. \end{aligned} \quad (12)$$

The emission angle θ defines as the photoelectron momentum $\mathbf{p}$ direction with respect to the molecular internuclear distance $\mathbf{R}$ axis. The total photoelectron distribution $\mathcal{F}(p, \theta, t)$ in equation (12) is composed of the two direct components, $\mathcal{F}^{(\sigma_g)}(p, \theta, t)$ and $\mathcal{F}^{(\sigma_u)}(p, \theta, t)$ respectively from the ground $1s\sigma_g$ and excited $2p\sigma_u$ electronic states, and their coherent superposition term, $\mathcal{F}^{(\sigma_g,\sigma_u)}(p, \theta, t)$.

As shown in figure 2, the photoionization at the time delay $\Delta\tau = -6\tau_1$ is initiated from the ground $1s\sigma_g$ electronic state by the x-ray probe pulse. The pump pulse does not influence the x-ray photoelectron emission. According to the ultrafast photoionization model in equation (12), the photoelectron distribution follows the form $\mathcal{F}^{(\sigma_g)}(p, \theta, t) \sim |c_{\sigma_g}(t)\cos(pR\cos\theta/2)\psi_{1s}(p)|^2$, since $c_{\sigma_u}(t) = 0$ at $t = 0$. With a $\lambda_2 = 5$ nm x-ray pulse, the corresponding photoelectron momentum is $p = \sqrt{2(\omega_2 - I_p)} = 4.01$ au and wavelength $\lambda_e = 2\pi/p = 1.57$ au. As a consequence of $\lambda_e < R$ [14], photoelectron diffraction occurs in the x-ray photoemission processes. As predicted in equation (12), the maxima of diffraction patterns occur at angles $(n \pm 0.21)\pi$, $n = 0, \pm 1, \pm 2, \cdots$. One can see that these angle nodes predicted from equation (12) are in good agreement with the numerical results in figure 2(a) and the x-ray photoelectron distributions show symmetric structure.

At the time delay $\Delta\tau = 6\tau_1$, the pump pulse switches off. The populations in the two electronic states are constant, $|c_{\sigma_u}(t)|^2 = |c_{\sigma_u}(t)|^2 = 0.5$ at $t > 11\tau_1$, also seen in figure 7(c). For both the electronic states, their photoelectron distributions, $\mathcal{F}^{(\sigma_g)}(p, \theta, t)$ and $\mathcal{F}^{(\sigma_u)}(p, \theta, t)$, are symmetric and do not depend on the time. The coherent superposition term $\mathcal{F}^{(\sigma_g,\sigma_u)}(p, \theta, t)$ leads to asymmetry of the photoelectron distributions. At $t = 12\tau_1$ one has $\cos(\Delta E t) = 1$ since $\Delta E\tau_1 = 2\pi$. As shown in equation (12), the interference term of the photoelectron distribution satisfies $\mathcal{F}^{(\sigma_g,\sigma_u)}(p, \theta = 0, t) = -\mathcal{F}^{(\sigma_g,\sigma_u)}(p, \theta = \pi, t)$. Consequently, asymmetric MFPADs are obtained in figure 2(b).

From equation (12) one can see that the coherent superposition term of the angular distributions of photoionization yields is dependent on the ionization time t, following $\cos(\Delta E t)$. Altering the ionization time t, i.e., the time delay $\Delta\tau$, gives rise to a periodic variance of the asymmetric x-ray MFPADs. To describe the periodical asymmetry of the MFPADs due to coherent excitation, we also introduce an asymmetry ratio Γ as the difference of probability between the forward and backward half of the momentum distribution at energy E_e, which can be defined as

$$\Gamma = \frac{\mathcal{J}_+^{E_e} - \mathcal{J}_-^{E_e}}{\mathcal{J}_+^{E_e} + \mathcal{J}_-^{E_e}}. \quad (13)$$

$\mathcal{J}_{\pm}^{E_e}$ present the distributions in forward (+) momentum direction $\mathcal{J}_+^{E_e} = \int_{-\pi/2}^{\pi/2} d\theta J^{E_e}(\theta)$ and backward (−) momentum directions $\mathcal{J}_-^{E_e} = \int_{\pi/2}^{3\pi/2} d\theta J^{E_e}(\theta)$, where $J^{E_e}(\theta)$ is obtained from equation (7).

Figure 3 illustrates the asymmetry ratio Γ at different time delays $\Delta\tau$. It is evident that as the time delay $\Delta\tau$ increases, the asymmetry of the MFPADs varies periodically as a cosine triangular function. At the time delay $\Delta\tau \approx 6.1\tau_1$, the distribution is mainly localized along the forward momentum direction (positive $\mathcal{J}_+^{E_e}$), whereas at $\Delta\tau \approx 6.6\tau_1$, the backward component (negative $\mathcal{J}_-^{E_e}$) dominates. The oscillation period is $\tau^{asy} = \tau_1$, the same as that of the coherent electron dynamics,

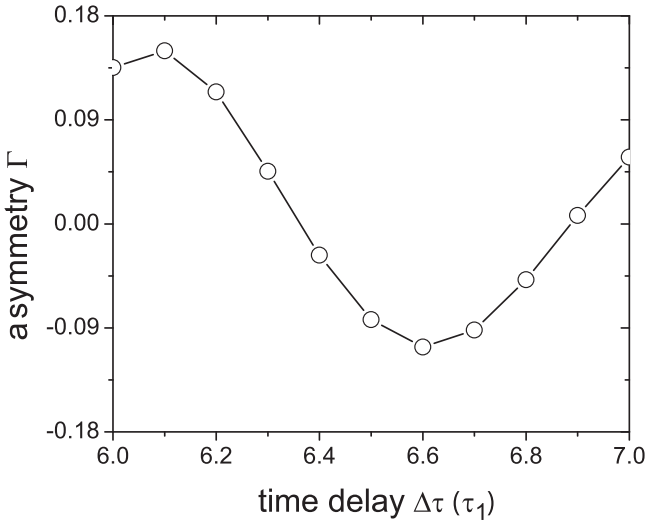

Figure 3. Dependence of the asymmetry parameter Γ between forward (positive) and backward (negative) momentum photoelectron distributions on the time-delayed $\Delta\tau$ in the molecular ion H_2^+, aligned along the x axis at $R = 2$ au by two-color $\lambda_1 = 100$ nm and $\lambda_2 = 5$ nm laser pulses, with their field vectors polarized along the molecular axis. The pulse intensities and durations are $I_{1/2} = 2.75 \times 10^{13}$ W cm^{-2} ($E_{1/2} = 2.8 \times 10^{-2}$ au), $T_{1/2} = 10\tau_{1/2}$, i.e., $T_1 = 3.31$ fs (1.655 fs FWHM) and $T_2 = 165.4$ as (83 as FWHM). The units $\tau_1 = 2\pi/\omega_1 = 331$ as.

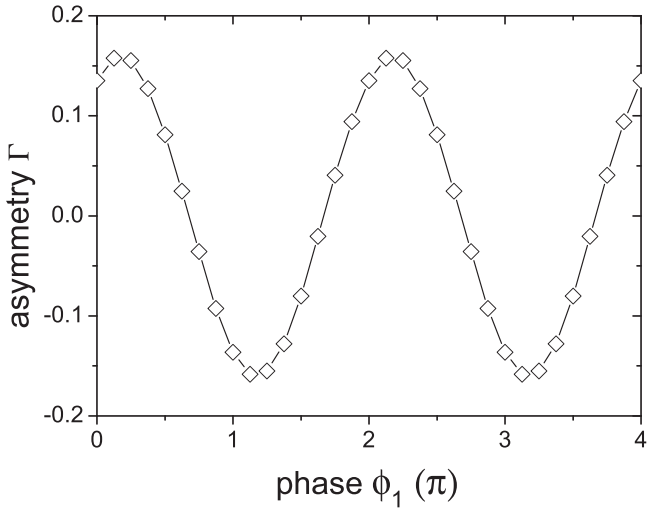

Figure 4. Dependence of the asymmetry parameter Γ between forward (positive) and backward (negative) momentum photoelectron distributions on the phase ϕ_1 in the coherent molecular excitation of H_2^+, aligned along the x axis at $R = 2$ au by two-color $\lambda_1 = 100$ nm and $\lambda_2 = 5$ nm laser pulses, with their field vectors polarized along the molecular axis. The time delay is $\Delta\tau = 6\tau_1$ i.e., the soft x-ray pulse $E_2(t)$ switches on after the XUV pump pulse $E_1(t)$. The pulse intensities and durations are $I_{1/2} = 2.75 \times 10^{13}$ W/cm^2 ($E_{1/2} = 2.8 \times 10^{-2}$ au), $T_{1/2} = 10\tau_{1/2}$, i.e., $T_1 = 3.31$ fs (1.655 fs FWHM) and $T_2 = 165.4$ as (83 as FWHM).

$2\pi/\Delta E = \tau_1 = 331$ as, predicted in the phase free equations (9) and (12). This confirms that the asymmetry of the MFPADs in figures 2(b) and 3 arises from the $\sigma_g - \sigma_u$ resonant excitation. The electron coherence leads to the time-dependent asymmetry of the MFPADs.

3.2. CEP-dependent symmetry

The asymmetry of the x-ray photoelectron distribution is also sensitive to the CEP of the pump pulse $\mathbf{E}_1(t)$. Figure 4 displays the dependence of the asymmetry parameter Γ on the phase ϕ_1 in the molecular H_2^+ aligned along the x axis by two-color $\lambda_1 = 100$ nm and $\lambda_2 = 5$ nm laser pulses. The time delay is fixed at $\Delta\tau = 6\tau_1$ i.e., the soft x-ray pulse $E_2(t)$ switches on after the XUV pump pulse $E_1(t)$. The phase of the soft x-ray pulse is $\phi_2 = 0$. One sees that varying the CEP ϕ_1 gives rise to an oscillation of the asymmetry Γ with a period of 2π. At $\phi_1 = (2n + 0.15)\pi$ and $(2n + 1.15)\pi$ the positive (forward) and negative (backward) photoelectron distributions dominate respectively. Around $\phi_1 = (n + 0.65)\pi$, x-ray photoionization yields show symmetric distributions where $\Gamma \approx 0$.

The effects of the CEP ϕ_1 of the pump pulse on the symmetry of the x-ray MFPADs illustrates the phase-dependent coherent resonant excitions in molecules. According to first order perturbation theory, the occupation coefficient c_{σ_u} in the excited state is defined as

$$c_{\sigma_u} = -i \int_{-\infty}^{t} dt' V_1(t') e^{i\Delta E t'}, \tag{14}$$

where $\Delta E = E_{\sigma_u} - E_{\sigma_g}$ is the energy difference between the two electronic states. The interaction term $V_1(t) = \langle \psi_{\sigma_g}(\mathbf{r}) | \mathbf{r} \cdot \mathbf{E}_1(t) | \psi_{\sigma_u}(\mathbf{r}) \rangle$ is a time-dependent matrix element, where the external pump field $\mathbf{E}_1(t) = \mathbf{e} E_1 e^{i(\omega_1 t + \phi_1)}$ includes the time factor t and the CEP ϕ_1 of the pulse $\mathbf{E}_1(t)$ [84]. The Fourier transform of the pulse, $E_1(\varepsilon) = \int E_1(t) e^{i\varepsilon t} dt$, in the frequency domain, is composed of two components, $\mathbf{E}_1(\varepsilon) = \mathbf{e}_\phi E_1^+(\varepsilon) + \mathbf{e}_\phi^* E_1^-(\varepsilon)$. The factors $E_1^\pm(\varepsilon)$ are CEP and polarization-independent scale parameters of the pulse $E_1^\pm(\varepsilon) = \frac{1}{2}\int E_1 e^{i(\varepsilon \mp \omega_1)t} dt$, $E_1^+(\varepsilon) = [E_1^-(-\varepsilon)]^*$, and the unit vector $\mathbf{e}_\phi = \mathbf{e} e^{i\phi_1}$. Therefore, the time-dependent excited state occupation coefficient c_{σ_u} in the superposition state in equation (8) is a function of the CEP of the pump pulse, which can be written as $c_{\sigma_u} = c'_{\sigma_u} e^{i\phi_1}$. The interfering superposition terms can be rewritten as

$$\mathcal{D}^{(g,u)}(\mathbf{r}, t) = 2|c_{\sigma_g}(t) c'_{\sigma_u}(t)| \psi_{\sigma_g}(\mathbf{r}) \psi_{\sigma_u}(\mathbf{r}) \cos(\phi_1 - \Delta E t), \tag{15}$$

for the time-dependent coherent electron density distribution and

$$\mathcal{F}^{(\sigma_g,\sigma_u)}(p, \theta, t) = |c_{\sigma_g}(t) c'_{\sigma_u}(t)| \sin(pR\cos\theta/2) \times \cos(\phi_1 - \Delta E t) |\psi_{1s}(p)|^2, \tag{16}$$

for the photoelectron momentum distribution. At $\phi_1 = 0$, equations (15) and (16) reduce to the corresponding phase-free results in equations (9) and (12). From equations (15) and (16) one notes that the asymmetry of the photoelectron distributions reflects the phase difference $\Delta\phi = \phi_1 - \Delta E t$. The information of the coherent electron state $\psi_c(\mathbf{r}, t)$ and $\mathcal{D}^{(g,u)}(\mathbf{r}, t)$ is imprinted on the photoionization yield $\mathcal{F}^{(\sigma_g,\sigma_u)}(p, \theta, t)$, which evolves as a function of the pump pulse phase ϕ_1 and the ionization time t, i.e., the time delay

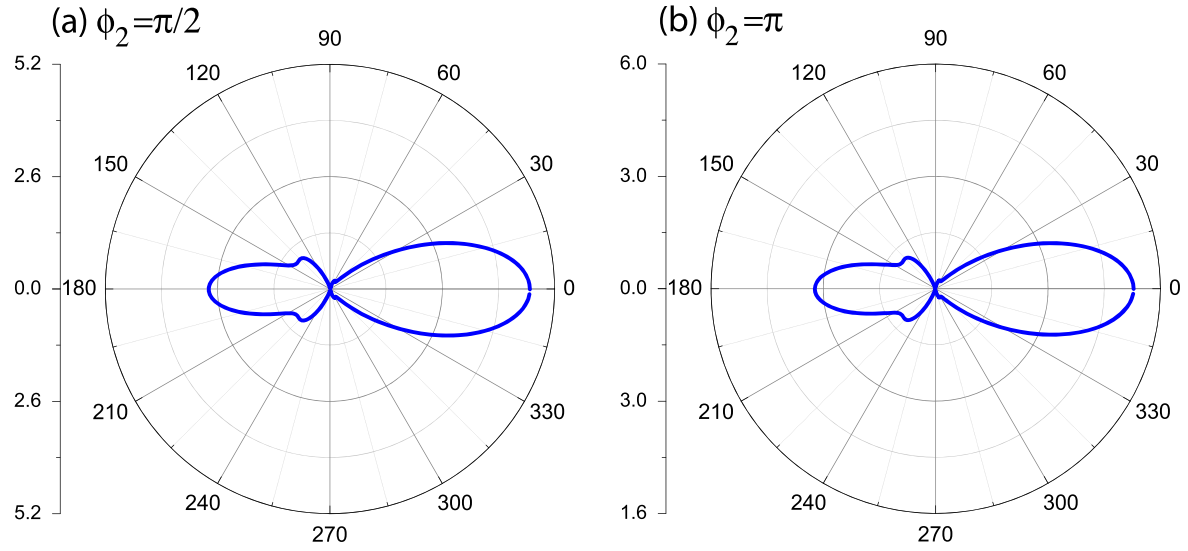

Figure 5. MFPADs of the molecular H_2^+ aligned along the x axis at $R = 2$ au by time-delayed two-color $\lambda_1 = 100$ nm and $\lambda_2 = 5$ nm laser pulses, with their field vectors polarized along the molecular axis. The probe-pulse phases ϕ_2 are, respectively, chosen as (a) $\pi/2$ and (b) π. The pump pulse CEP is $\phi_1 = 0$. The time delay is fixed at $\Delta\tau = 6\tau_1$. The pulse intensities and durations are $I_{1/2} = 2.75 \times 10^{13}$ W cm^{-2} ($E_{1/2} = 2.8 \times 10^{-2}$ au), $T_{1/2} = 10\tau_{1/2}$, i.e., $T_1 = 3.31$ fs (1.655 fs FWHM) and $T_2 = 165.4$ as (83 as FWHM). Arbitrary units of MFPADs are used.

$\Delta\tau$. As a result, varying the CEP ϕ_1 leads to a modulation of the asymmetry of the MFPADs in figure 4.

For comparison we also present the CEP ϕ_2 effects of the soft x-ray probe pulse on the asymmetry of the MFPADs. Figure 5 shows the results of the MFPADs at different phases (a) $\phi_2 = \pi/2$ and (b) π. The CEP of the pump pulse and the time delay are fixed at $\phi_1 = 0$ and $\Delta\tau = 6\tau_1$. The other laser parameters are the same as those used in figure 4. It is found that the MFPADs exhibit the same asymmetric structure for both CEPs ϕ_2, as obtained in figure 2(a) at $\phi_2 = 0$. Varying the CEP ϕ_2 does not influence the asymmetry of the photoionization yields, confirming that the signature of the asymmetry of the MFPADs arises from the molecular coherent excitation induced by the pump pulse $\mathbf{E}_1(t)$. The forward ($\theta = 0$) asymmetry is indicative of charge localization on the right-hand proton [47].

3.3. Influence of the pulse intensity and duration on the asymmetry of MFPADs

We next present the effects of the pulse intensity on the asymmetry of the x-ray photoelectron distributions. Figure 6 displays the MFPADs at different field strengths of the pump pulse: (a) $E_1 = 0.25E_0$ ($I_1 = 1.72 \times 10^{12}$ W cm^{-2}), (b) $0.5E_0$ (6.88×10^{12} W cm^{-2}), (c) $2.0E_0$ (1.1×10^{14} W cm^{-2}), and (d) $4.0E_0$ (4.4×10^{14} W cm^{-2}), where $E_0 = 2.8 \times 10^{-2}$ au ($I_0 = 2.75 \times 10^{13}$ W cm^{-2}). We fix the probe-pulse intensity at $I_2 = I_0$ ($E_2 = E_0$). The CEPs and the time delay are $\phi_1 = \phi_2 = 0$ and $\Delta\tau = 6.0\tau_1$. The other laser parameters are the same those used in figures 2–5. It is found that the MFPADs are strongly modulated by the pump pulse intensity I_1 (E_1). At $E_1 = 0.25E_0$ the MFPADs exhibit four angular nodes which are asymmetric in the left–right planes. The distributions dominate in the right plane. As the pulse intensity increases, the asymmetry increases. The maximum asymmetry occurs at E_0 in figure 2(b). Increasing the pulse intensity further, the asymmetry of the MFPADs decreases. At $E_1 = 2.0E_0$ and $4.0E_0$, one sees that the MFPADs in the left and right planes are nearly equal in amplitude, as displayed in figures 6(c) and (d). This modulation mainly comes from the change of amplitudes of the coherent excitation, i.e., the increase in ionization rate being faster than the slower charge migration time scale illustrated in figure 7.

As shown in equation (16), the amplitudes of the coherent electron wave packets, $c_{\sigma_g}(t)$ and $c'_{\sigma_u}(t)$, can also lead to a modulation of the photoelectron distributions. In figure 7 we show the evolutions of the population in the ground $1s\sigma_g$ and the excited $2p\sigma_u$ electronic states of the $x-$aligned molecular ion H_2^+ with time t at different pump pulse intensities, corresponding to figure 6, where

$$|c_{\sigma_{g/u}}(t)| = |\langle\psi_{\sigma_{g/u}}(\mathbf{r})|\psi(\mathbf{r}, t)\rangle|, \tag{17}$$

with the eigenfunction $\psi_{\sigma_{g/u}}(\mathbf{r})$ of the $1s\sigma_g/2p\sigma_u$ electronic state and the electron wavefunction $\psi(\mathbf{r}, t)$ obtained from equation (1). The different population evolutions reflect various coherent excitation processes. The excitation probability reads as

$$|c'_{\sigma_u}(t)|^2 = |\sin[A(t)/2]|^2, \tag{18}$$

where the pulse area $A(t)$ is

$$A(t) = \mu E_1 \int_{-\infty}^{t} f_1(t')dt', \tag{19}$$

with the transition dipole matrix element μ between the two resonant electronic states. The population undergoes triangular function variation. For the weak field cases, the corresponding numerical populations $|c_{\sigma_g}(t)|^2$ and $|c'_{\sigma_u}(t)|^2$ are 0.05 and 0.95 at $E_1 = 0.25E_0$, and 0.18 and 0.82 at $E_1 = 0.5E_0$ after the pump pulses ($t > 11\tau_1$), due to the small

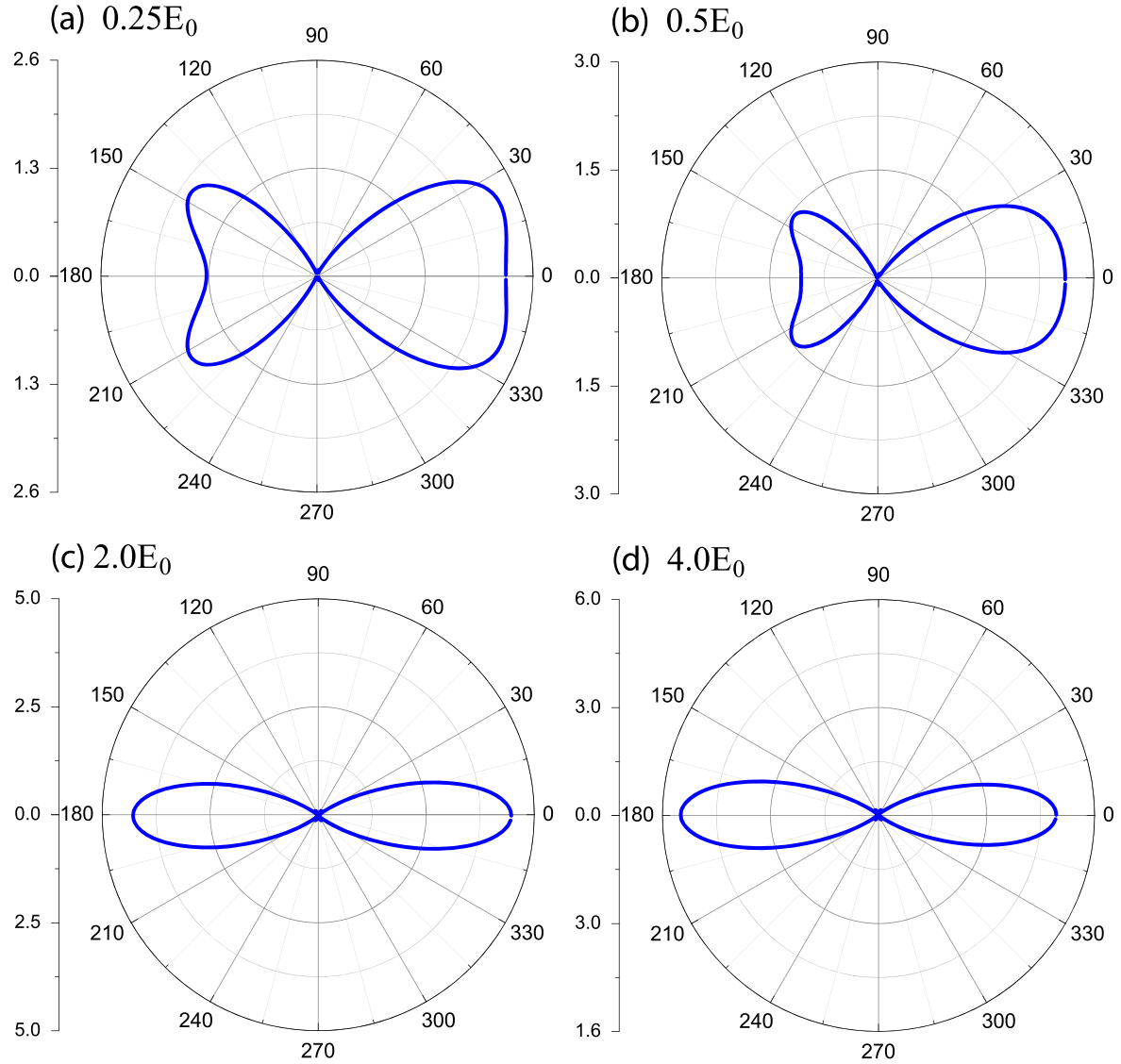

Figure 6. MFPADs at different pulse strengths of the pump pulse (a) $E_1 = 0.25E_0$ ($I_1 = 1.72 \times 10^{12}$ W cm^{-2}), (b) $0.5E_0$ (6.88×10^{12} W cm^{-2}), (c) $2.0E_0$ (1.1×10^{14} W cm^{-2}), and (d) $4.0E_0$ (4.4×10^{14} W cm^{-2}), where $I_0 = 2.75 \times 10^{13}$ W cm^{-2} ($E_0 = 2.8 \times 10^{-2}$ au). The molecular H_2^+ is aligned along the x axis at $R = 2$ au. The time delay between the two pulses, pump $E_1(t)$ and probe $E_2(t)$, is $\Delta\tau = 6.0\tau_1$ (2 fs). The pulse durations are $T_{1/2} = 10\tau_{1/2}$, i.e., $T_1 = 3.31$ fs (1.655 fs FWHM) and $T_2 = 165.4$ as (83 as FWHM). The intensity of the probe pulse is fixed at $I_2 = I_0$ ($E_2 = E_0$). Arbitrary units of MFPADs are used.

interaction term of μE_1. The σ_g dominant photoionization leads to four angular nodes in the MFPADs. As the coefficient $|c_{\sigma_g} c'_{\sigma_u}|$ increases, the interference effect enhances, giving rise to an enhancement of the asymmetry in the MFPADs. The maximum appears at $|c_{\sigma_g}|^2 = |c'_{\sigma_u}|^2 = 0.5$. At $E_1 = 2.0E_0$, the population $|c_{\sigma_g}(t)|^2$ in the ground $1s\sigma_g$ state is reduced due to ionization. We also note that at $E_1 = 4E_0$, pronounced Rabi oscillations of population are induced during the pump process. The population in the intermediate resonant excited $2p\sigma_u$ state decreases and the ground $1s\sigma_g$ state population recovers. The Rabi frequency is $\Omega = \mu E_1$, i.e., the oscillation period is defined by $\tau_{ra} = 2\pi/\mu E_1$. For example, at $E_1 = 4.0E_0$, the Rabi frequency is $\Omega = 0.112$ au and the corresponding oscillation period is $\tau_{ra} = 2\pi/\Omega = 56.07$ au, $\approx 4.1\tau_1$, with $\mu = R/2 = 1.0$ au for the $1s\sigma_g - 2p\sigma_u$ transition moment of H_2^+ [76]. The numerical results in figure 7(e) agree well with the prediction values. Due to ionization effects, the amplitudes of the Rabi oscillation decreased gradually. As shown in figure 7(e), the state populations are $|c_{\sigma_g}|^2 = 0.22$ and $|c'_{\sigma_u}|^2 = 0.09$, after the pump pulse $t > 11\tau_1$. In these cases with strong pulse intensities, the coherent effects becomes suppressed, thus resulting in approximately symmetric MFPADs in figures 6(c) and (d).

According to the pulse area theorem in equations (18) and (19), similar phenomena should be produced at different pulse durations T_1 of the XUV pump pulse $\mathbf{E}_1(t)$. Altering T_1 modifies the coherent resonant excitation, thus varying the asymmetry of the MFPADs. Moreover, it should be noted that the asymmetry of the MFPADs is not sensitive to the pulse intensity I_2 of the soft x-ray probe pulse $\mathbf{E_2}(t)$. The amplitude of the MFPADs is determined mainly by the probe-pulse

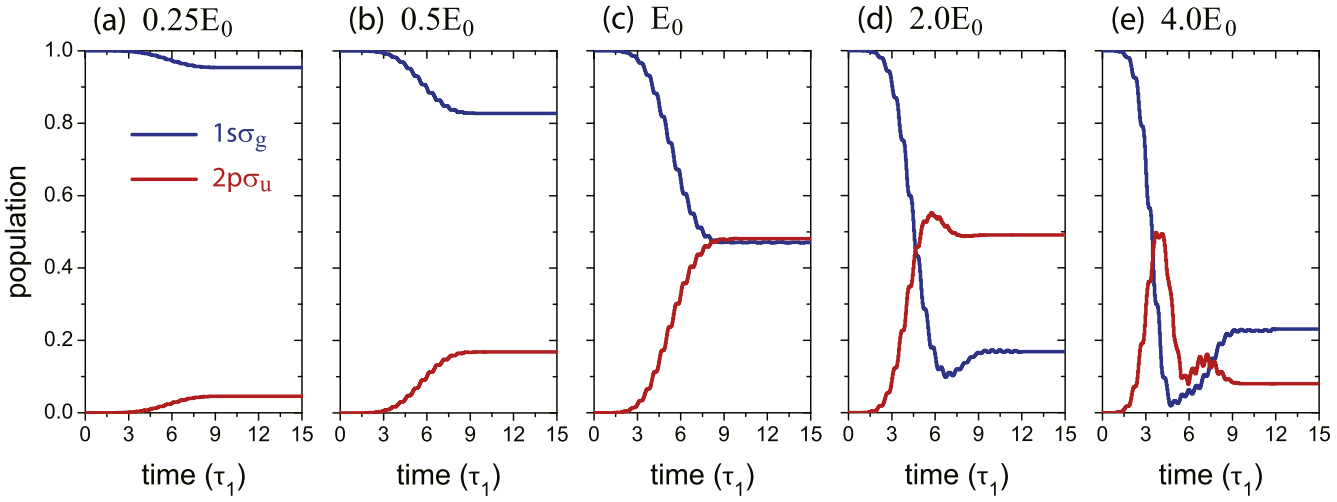

Figure 7. Evolutions of population in the ground $1s\sigma_g$ (black) and excited $2p\sigma_u$ (red) electronic states at different electric field strengths E_1 and $E_2 = E_0$. The molecular ion H_2^+ is aligned along the x axis at $R = 2$ au. The time delay between the two pulses $E_1(t)$ and $E_2(t)$ is $\Delta\tau = 6.0\tau_1$ (2 fs). The intensity is defined as $I_0 = 2.75 \times 10^{13}$ W cm^{-2} ($E_0 = 2.8 \times 10^{-2}$ au). The durations of the pump-probe pulses are $T_{1/2} = 10\tau_{1/2}$, i.e., $T_1 = 3.31$ fs (1.655 fs FWHM) and $T_2 = 165.4$ as (83 as FWHM), c.f., figure 6.

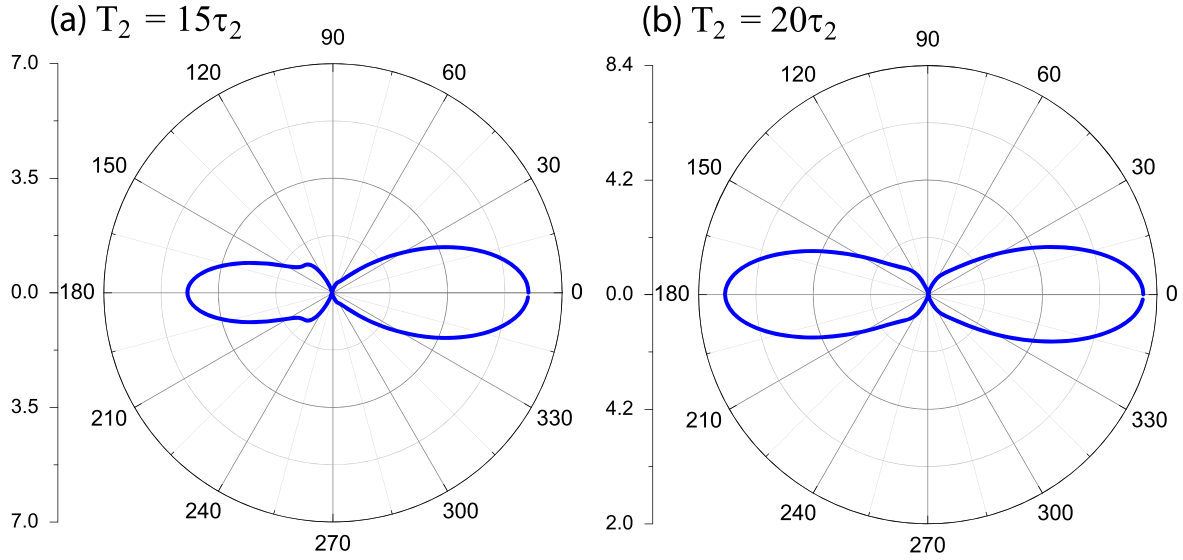

Figure 8. MFPADs at different durations of the probe pulse $E_2(t)$: (a) $T_2 = 15\tau_2 = 248.1$ as (124 as FWHM) and $20\tau_2 = 330.8$ as (166 as FWHM). The molecular H_2^+ is aligned along the x axis. The time delay between the two pulses $E_1(t)$ and $E_2(t)$ is $\Delta\tau = 6.0\tau_1$ (2 fs), the pulse intensities are $I_{1/2} = 2.75 \times 10^{13}$ W cm^{-2} ($E_{1/2} = 2.8 \times 10^{-2}$ au), the duration of the pump pulse $E_1(t)$ is $T_1 = 10\tau_1$, i.e., $T_1 = 3.31$ fs (1.655 fs FWHM), and CEPs $\phi_1 = \phi_2 = 0$. Arbitrary units of MFPADs are used.

intensity. The change of I_2 does not influence of the coherent electron dynamics in the molecule H_2^+.

We finally present the pulse duration effects of the probe pulse on the asymmetry of the MFPADs. Figure 8 displays the MFPADs of the molecular H_2^+ aligned along the x axis at different durations of the soft x-ray probe pulse $E_2(t)$, (a) $T_2 = 15\tau_2 = 248.1$ as (124 as FWHM) and (b) $20\tau_2 = 330.8$ as (166 as FWHM). We fix the duration of the pump pulse $T_1 = 10\tau_1$, i.e., $T_1 = 3.31$ fs (1.655 fs FWHM), the time delay between $\Delta\tau = 6.0\tau_1$ (2 fs), and the pulse intensity $I_{1/2} = 2.75 \times 10^{13}$ W cm^{-2} ($E_{1/2} = 2.8 \times 10^{-2}$ au), corresponding to figure 2(b). The results in figures 2(b) and 8 show that the symmetry of the MFPADs is also dependent on the duration of the probe pulse. With a long probe-pulse duration, symmetric distributions are produced.

As predicted in equations (8), (9) and (12), the photoionization yield comes from the time-dependent coherent superposition state. The time dependence of the MFPADs illustrates the evolution of the CEWPs in molecules. The period of the coherent or charge migration electron motion is $\tau^{co} = 2\pi/\Delta E = \tau_1 = 13.8$ au $= 331$ as. For long duration of the probe pulse, since $T_2 > \tau^{co} = \tau_1$, the averaged density probabilities of the coherent superposition state are symmetric during the probe processes. As a result, the time evolution of the electron between the protons cannot be tracked by time-resolved MFPADs. The photoelectron distributions are

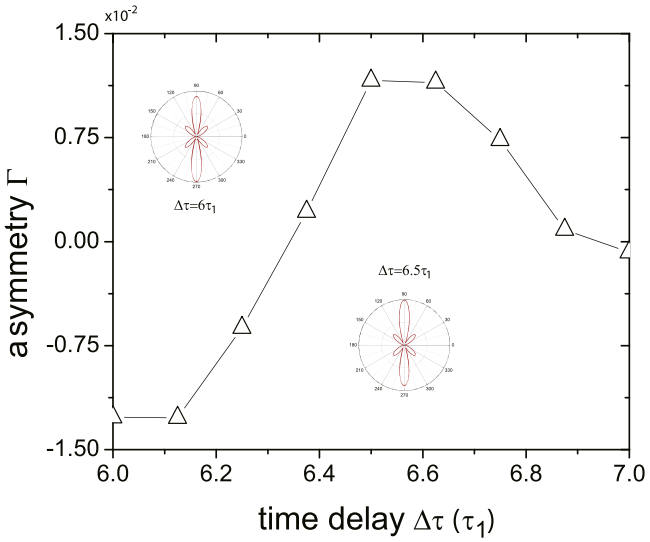

Figure 9. Dependence of the asymmetry parameter Γ between positive ($p_y > 0$) and negative ($p_y < 0$) momentum photoelectron distributions on the time-delayed $\Delta\tau$ in the $\sigma_g - \pi_u$ perpendicular transition, in the molecular ion H_2^+ aligned along the x axis at $R = 2$ au by two-color $\lambda_1 = 70$ nm and $\lambda_2 = 5$ nm laser pulses, with their field vectors polarized perpendicular to the molecular axis. The pulse intensities and durations are $I_{1/2} = 5.0 \times 10^{13}$ W cm^{-2} ($E_{1/2} = 3.8 \times 10^{-2}$ au), $T_{1/2} = 10\tau_{1/2}$, i.e., $T_1 = 2.21$ fs (1.105 fs FWHM) and $T_2 = 165.4$ as (83 as FWHM). The units $\tau_1 = 2\pi/\omega_1 = 221$ as. Inserts are MFPADs at time delays $\Delta\tau = 6.0\tau_1$ and $6.5\tau_1$.

simply the sum of the distributions originated from the ground state and the excited electronic state, as shown in equation (12) $\mathcal{F}(p, \theta, t) = \mathcal{F}^{(\sigma_g)}(p, \theta, t) + \mathcal{F}^{(\sigma_u)}(p, \theta, t)$, and figure 8(b). The dependence of the MFPAD on the probe-pulse duration confirms that the asymmetry results from the coherent resonant excitation by the pump pulse, and the importance of the short duration and high frequency of the probe pulse in the dynamical reconstruction of coherent excitation processes.

3.4. Asymmetry of MFPADs in perpendicular $\sigma_g - \pi_u$ transitions

Figures 2–8 show results of the $\sigma_g - \sigma_u$ transition. Similar asymmetry of the MFPADs can also be obtained in the perpendicular $\sigma_g - \pi_u$ transition. Figure 9 shows the asymmetry parameter Γ of MFPADs at different time delays $\Delta\tau$ from equation (13), where the distributions in positive (+) and negative (−) momentum directions define as $\mathcal{J}_+^{E_e} = \int_0^{\pi} d\theta J^{E_e}(\theta)$ for $p_y > 0$ and $\mathcal{J}_-^{E_e} = \int_{\pi}^{2\pi} d\theta J^{E_e}(\theta)$, where $J^{E_e}(\theta)$ is obtained from equation (7). A $\lambda_1 = 70$ nm ($\omega_1 = 0.65$ au) pump pulse with its field vector polarized along the y axis, perpendicular to the molecular R axis, is used to excited the molecule H_2^+. Subsequently, a linearly polarized 5 nm soft x-ray probe pulse with its field vector polarized along the y axis is employed to ionize the excited molecule. The pulse intensities and durations are $I_{1/2} = 5.0 \times 10^{13}$ W cm^{-2} ($E_{1/2} = 3.8 \times 10^{-2}$ au), $T_{1/2} = 10\tau_{1/2}$, i.e., $T_1 = 2.21$ fs (1.105 fs FWHM) and $T_2 = 165.4$ as (83 as FWHM). The corresponding MFPADs at time delays $\Delta\tau = 6.0\tau_1$ and $6.5\tau_1$ are also plotted, with reverse asymmetries. From figure 9 one can see that the asymmetry ratio Γ varies with the time delay $\Delta\tau$.

Since $\omega_1 = \Delta E' = E_{\pi_u} - E_{\sigma_g}$, the energy difference between the $1s\sigma_g$ and $2p\pi_u$ electronic states, a resonant excitation occurs, leading to a coherent superposition of the two electronic states,

$$\psi_c'(\mathbf{r}, t) = c_{\sigma_g}(t)\psi_{\sigma_g}(\mathbf{r})e^{-iE_{\sigma_g}t} + c_{\pi_u}(t)\psi_{\pi_u}(\mathbf{r})e^{-iE_{\pi_u}t}, \quad (20)$$

with the occupation coefficient $c_{\pi_u}(t)$ and eigenfuntion $\psi_{\pi_u}(\mathbf{r})$ of the excited $2p\pi_u$ state. According to the ultrafast photoionization model [14], the corresponding photoemission yields, MFPADs, of the superposition state $\psi_c'(\mathbf{r}, t)$, read as

$$\begin{aligned}\mathcal{F}'(\mathbf{p}, t) \sim & |c_{\sigma_g}(t)\cos[(\mathbf{P} + \mathbf{F}) \cdot \mathbf{R}/2]\psi_{1s}(\mathbf{P} + \mathbf{F})|^2 \\ & + |c_{\pi_u}(t)\cos[(\mathbf{P} + \mathbf{F}) \cdot \mathbf{R}/2]\psi_{2p}(\mathbf{P} + \mathbf{F})|^2 \\ & + |c_{\sigma_g}(t)c_{\pi_u}(t)|\{1 + \cos[(\mathbf{P} + \mathbf{F}) \cdot \mathbf{R}]\} \\ & \times \cos(\Delta E' t)\psi_{1s}(\mathbf{P} + \mathbf{F})\psi_{2p}(\mathbf{P} + \mathbf{F}).\end{aligned} \quad (21)$$

Equation (21) shows that total MFPADs $\mathcal{F}'(\mathbf{p}, t)$ are asymmetric and vary as a function of t. Therefore, altering the time delay $\Delta\tau$ gives rise to a modulation of the MFPADs and the asymmetry ratio evolves periodically, i.e., $\Gamma \sim \cos(\Delta E'\Delta\tau)$, as illustrated in figure 9. The corresponding oscillation period should be $2\pi/\Delta E' = 221$ as, the prediction in equation (21). For instance, at time delay $\Delta\tau = 6.0\tau_1$, the asymmetry parameters are $\Gamma = -1.48 \times 10^{-2}$ and 1.35×10^{-2} at $\Delta\tau = 6.5\tau_1$. However, at $\Delta\tau = 7.0\tau_1$, $\Gamma = -0.1 \times 10^{-2}$. The asymmetry ratio is weaker than the expected value. For the $\sigma_g - \pi_u$ excitation, the interfering term is very weak with small transition probabilities $|c_{\pi_u}(t)|^2$ and transition dipole moments $\mu_{\sigma_g\pi_u}$. As a result, at larger time delays, the asymmetry of the MFPADs decreases due to the spread of the coherent electron wave packets.

From equation (21) it can also be found that the asymmetry of the MFPADs in the $\sigma_g - \pi_u$ resonant transition is also dependent on the laser parameters of the pump-probe laser pulse, similar to those presented in figures 2–8 for the $\sigma_g - \sigma_u$ transition. Varying the phase, duration and intensity of the pump pulse results in a modulation of the asymmetry of the MFPADs. The asymmetry does not depend on the intensity and phase of the probe pulse. Due to the attosecond resolution of the coherent electron wave packet, the asymmetric MFPADs are sensitive to the duration of the probe pulse, and disappear at long pulse durations.

4. Conclusions

We present photoionization of the molecule H_2^+ by intense two-color ultrashort laser pulses from numerical solutions of corresponding TDSEs. A soft x-ray 5 nm attosecond probe pulse is used to ionize the molecular target in the presence of a 100/70 nm XUV pump field. Simulation results show that the MFPADs exhibit a signature of time-dependent asymmetry with a time-delay between the two pulses, thus allowing the exploration of coherent excitation and charge

migration [71]. It is found that the asymmetry is also dependent on the phase and intensity of the pump pulse and the duration of the probe pulse. The dependence reflects the time-dependence of the coherent excitation in molecules.

The XUV pump pulse leads to a coherent superposition, $\psi_c(\mathbf{r}, t)$, between the ground $1s\sigma_g$ and excited $2p\sigma_u$ electron states in the molecule H_2^+ by 100 nm pump pulses. The corresponding CEWPs evolve with time between the two nuclei, as predicted in equation (9). By a soft x-ray attosecond probe pulse, photoionization yields initiating from the coherent superposition state show asymmetric MFPADs. We introduce a parameter Γ to describe the asymmetric MFPADS. The results show that:

- The asymmetry ratio Γ is a function of the time delay between the pump-probe pulses, reflecting the coherent superposition of electronic states, i.e., $\Gamma \sim \Delta\tau$. The time-resolved photoelectron distributions illustrate the CEWP motion, giving rise to charge migration following the form $\cos(\Delta E t)$ in equation (12) and figure 3. Therefore, the asymmetry ratio evolves with a period of $2\pi/\Delta E$.
- The asymmetry ratio Γ depends on the the phase of the pump pulse, i.e., $\Gamma \sim \phi_1$. The evolution of CEWPs is sensitive to the phase of the pump pulse. Consequently, varying the pulse CEP induces a periodic oscillation of the asymmetry of MFPADs.
- The asymmetry ratio Γ is sensitive to the intensity and duration of the pump pulse, i.e., $\Gamma \sim E_1$ or T_1, $\sim c_{\sigma_g} c_{\sigma_u}$. The coherent superposition of the two electronic states is determined by the orbital occupation coefficients, c_{σ_g} and c_{σ_u}, as shown in equation (8). Altering the intensity of the pump pulse thus gives rise to a modulation of the asymmetric MFPADs due to varying orbital populations. At lower intensities, the excitation is weaker and the ionization from the ground $1s\sigma_g$ state dominates. Pronounced photoelectron diffraction patterns are obtained in MFPADs. The maximum asymmetry occurs in the case of $|c_{\sigma_g}|^2 = |c_{\sigma_u}|^2 = 0.5$ which corresponds to maximum charge localization [47]. For the processes at higher intensities, Rabi oscillations are induced and ionization is enhanced, suppressing the asymmetry of MFPADs.
- The asymmetry ratio Γ varies with the duration of the probe pulse, i.e., $\Gamma \sim T_2$. For long duration probe pulses the asymmetry of the MFPADs disappears due to the symmetry of the averaged density distributions of the oscillating coherent state population.

Similar dynamics are produced in the coherent resonant excitation process between the ground $1s\sigma_g$ and excited $2p\pi_u$ electron states by 70 nm pump pulses, as illustrated in figure 9. It also found that due to the spread of CEWPs, the asymmetry is suppressed at large time delays.

The present demonstration in principle paves the way for a new method for tracking coherent excitation processes in molecules by intense ultrafast laser pulses. The dependence of the asymmetry of photoemission yields on these parameters, such as time delay, phase, intensity and duration of the pump and probe pulses allows us to characterize the coherent electron dynamics processes. Similar ultrafast phenomena should be predicted in more complex molecular systems, thus offering a possibility for measuring molecular coherent excitation and charge migration from ultrafast x-ray photoionization [85–87].

Acknowledgments

The authors thank Compute Canada for access to massively parallel computer clusters, and the Natural Sciences and Engineering Research Council of Canada (NSERC) and the Fonds de Recherche du Québec—Nature et Technologies (FRQNT) for partially supporting their research work. KJY would also like to acknowledge support from the National Natural Science Foundation of China under Grant No. 11974007.

ORCID iDs

Kai-Jun Yuan https://orcid.org/0000-0002-0338-6995

References

[1] Krausz F and Ivanov M 2009 Attosecond physics *Rev. Mod. Phys.* **81** 163
[2] Chang Z, Corkum P and Leone S R 2016 Attosecond optics and technology: progress to date and future prospects *J. Opt. Soc. Am.* B **33** 1081
[3] Baum P and Krausz F 2017 Capturing atomic-scale carrier dynamics with electrons *Chem. Phys. Lett.* **683** 57
[4] Nisoli M, Decleva P, Calegari F, Palacios A and Martin F 2017 Attosecond electron dynamics in molecules *Chem. Rev.* **117** 10760
[5] Krüger M, Lemell C, Wachter G, Burgdörfer J and Hommelhoff P 2018 Attosecond physics phenomena at nanometric tips *J. Phys. B: At. Mol. Opt. Phys.* **51** 172001
[6] Gaumnitz T, Jain A, Pertot Y, Huppert M, Jordan I, Ardana-Lamas F and Wörner H J 2017 Streaking of 43-attosecond soft-x ray pulses generated by a passively CEP-stable mid-infrared driver *Opt. Express* **25** 27506
[7] Zewail A H 2000 Femtochemistry: atomic-scale dynamics of the chemical bond *J. Phys. Chem. A.* **104** 5660
[8] Stolow A, Bragg A E and Neumark D M 2004 Femtosecond time-resolved photoelectron spectroscopy *Chem. Rev.* **104** 1719
[9] Reid K L 2008 Picosecond time-resolved photoelectron spectroscopy as a means of gaining insight into mechanisms of intramolecular vibrational energy redistribution in excited states *Int. Rev. Phys. Chem.* **27** 607
[10] Arasaki Y, Takatsuka K, Wang K and McKoy V 2010 Time-resolved photoelectron spectroscopy of wavepackets through a conical intersection in NO_2 *J. Chem. Phys.* **132** 124307
[11] Douguet N, Rescigno T N and Orel A E 2012 Time-resolved molecular-frame photoelectron angular distributions: Snapshots of acetylene-vinylidene cationic isomerization *Phys. Rev.* A **86** 013425
[12] Kammrath A, Griffin G B, Verlet J R R, Young R M and Neumark D M 2007 Time-resolved photoelectron imaging

of large anionic methanol clusters:$(methanol)_n$ (n ∼ 145535) *J. Chem. Phys.* **126** 244306
[13] Svoboda V, Ram N B, Rajeev R and Wörner H J 2017 Time-resolved photoelectron imaging with a femtosecond vacuum-ultraviolet light source: dynamics in the A/B and F-bands of SO_2 *J. Chem. Phys.* **146** 084301
[14] Zuo T, Bandrauk A D and Corkum P B 1996 Laser-induced electron diffraction: a new tool for probing ultrafast molecular dynamics *Chem. Phys. Lett.* **259** 313
[15] Yurchenko S N, Patchkovskii S, Litvinyuk I V, Corkum P B and Yudin G L 2004 Laser-induced interference, focusing, and diffraction of rescattering molecular photoelectrons *Phys. Rev. Lett.* **93** 223003
[16] Bian X B and Bandrauk A D 2012 Attosecond time-resolved imaging of molecular structure by photoelectron holography *Phys. Rev. Lett.* **108** 263003
[17] Pullen M G *et al* 2015 Imaging an aligned polyatomic molecule with laser-induced electron diffraction *Nature Commun.* **6** 7262
[18] Meckel M *et al* 2008 Laser-induced electron tunneling and diffraction *Science* **320** 1478
[19] Peters M, Nguyen-Dang T T, Charron E, Keller A and Atabek O 2012 Laser-induced electron diffraction: A tool for molecular orbital imaging *Phys. Rev.* A **85** 053417
[20] Puthumpally-Joseph R, Viau-Trudel J, Peters M, Nguyen-Dang T T, Atabek O and Charron E 2016 Inversion of strong-field photoelectron spectra for molecular orbital imaging *Phys. Rev.* A **94** 023421
[21] Nguyen-Dang T T, Peters M, Viau-Trudel J, Couture-Bienvenue E, Puthumpally-Joseph R, Charron E and Atabek O 2017 Laser-induced electron diffraction: alignment defects and symmetry breaking *Mol. Phys.* **115** 1934
[22] Aidelsburger M, Kirchner F O, Krausz F and Baum P 2010 Single-electron pulses for ultrafast diffraction *Proc. Natl. Acad. Sci. U.S.A.* **107** 19714
[23] Huismans Y *et al* 2011 Time-resolved holography with photoelectrons *Science* **331** 61
[24] Porat G *et al* 2018 Attosecond time-resolved photoelectron holography *Nature Commun.* **9** 2805
[25] Amini K *et al* 2019 Imaging the renner-teller effect using laser-induced electron diffraction *Proc. Natl. Acad. Sci. U.S.A.* **116** 8173
[26] Kim H L and Bersohn R 1997 Control of photofragment angular distribution by laser phase variation *J. Chem. Phys.* **107** 4546
[27] Vrakking M J J and Stolte S 1997 Coherent control of molecular orientation *Chem. Phys. Lett.* **271** 209
[28] Aubanel E E and Bandrauk A D 1994 Orbital alignment and electron control in photodissociation products by two-color laser interference *Chem. Phys. Lett.* **229** 169
[29] Wang Z M and Elliott D S 2001 Determination of the phase difference between even and odd continuum wave functions in atoms through quantum interference measurements *Phys. Rev. Lett.* **87** 173001
[30] Yin Y Y, Chen C, Elliott D S and Smith A V 1992 Asymmetric photoelectron angular distributions from interfering photoionization processes *Phys. Rev. Lett.* **69** 2353
[31] Yuan K J and Bandrauk A D 2012 Molecular above-thresholdionization angular distributions with attosecond bichromatic intense XUV laser pulses *Phys. Rev.* A **85** 013413
[32] Grum-Grzhimailo A N, Gryzlova E V, Staroselskaya E I, Venzke J and Bartschat K 2015 Interfering one-photon and two-photon ionization by femtosecond VUV pulses in the region of an intermediate resonance *Phys. Rev.* A **91** 063418
[33] Yuan K J and Bandrauk A D 2016 Interference asymmetry of molecular frame photoelectron angular distributions in bichromatic UV ionization processes *J. Phys. B: At. Mol. Opt. Phys.* **49** 065601
[34] Chamakhi R, Telmini M, Atabek O and Charron E 2019 Anisotropy control in photoelectron spectra: a coherent two-pulse interference strategy *Phys. Rev.* A **100** 033402
[35] Hu W, Liu Y, Luo S, Li X, Yu J, Li X, Sun Z, Yuan K J, Bandrauk A D and Ding D 2019 Coherent interference of molecular electronic states in NO by two-color femtosecond laser pulses *Phys. Rev.* A **99** 011402
[36] Liu Y, Hu W, Luo S, Yuan K J, Sun Z, Bandrauk A D and Ding D 2019 Vibrationally resolved above-threshold ionization in NO molecules by intense ultrafast two-color laser pulses: An experimental and theoretical study *Phys. Rev.* A **100** 023404
[37] Ngoko Djiokap J M, Hu S X, Madsen L B, Manakov N L, Meremianin A V and Starace A F 2015 Electron vortices in photoionization by circularly polarized attosecond pulses *Phys. Rev. Lett.* **115** 113004
[38] Ngoko Djiokap J M, Meremianin A V, Manakov N L, Hu S X, Madsen L B and Starace A F 2016 Multistart spiral electron vortices in ionization by circularly polarized UV pulses *Phys. Rev.* A **94** 013408
[39] Ngoko Djiokap J M, Meremianin A V, Manakov N L, Madsen L B, Hu S X and Starace A F 2018 Dynamical electron vortices in attosecond double photoionization of H_2 *Phys. Rev.* A **98** 063407
[40] Pengel D, Kerbstadt S, Johannmeyer D, Englert L, Bayer T and Wollenhaupt M 2017 Electron vortices in femtosecond multiphoton ionization *Phys. Rev. Lett.* **118** 053003
[41] Li M, Zhang G, Kong X, Wang T, Ding X and Yao J 2018 Dynamic Stark induced vortex momentum of hydrogen in circular fields *Opt. Express* **26** 878
[42] Yuan K J, Chelkowski S and Bandrauk A D 2016 Photoelectron momentum distributions of molecules in bichromatic circularly polarized attosecond UV laser fields *Phys. Rev.* A **93** 053425
[43] Yuan K J, Lu H and Bandrauk A D 2017 Photoionization of triatomic molecular ions H_3^{2+} by intense bichromatic circularly polarized attosecond UV laser pulses *J. Phys. B: At. Mol. Opt. Phys.* **50** 124004
[44] Jia J, Cui H, Zhang C, Shao J, Ma J and Miao X 2019 Investigation of the photoionization process of helium ion in bichromatic circularly XUV fields with different time delays *Chem. Phys. Lett.* **725** 119
[45] Yuan K J, Shu C C, Dong D and Bandrauk A D 2017 Attosecond dynamics of molecular electronic ring currents *J. Phys. Chem. Lett.* **8** 2229
[46] Yuan K J and Bandrauk A D 2019 Probing attosecond electron coherence in molecular charge migration by ultrafast X-Ray photoelectron imaging *Appl. Sci.* **9** 1941
[47] Yudin G L, Chelkowski S, Itatani J, Bandrauk A D and Corkum P B 2005 Attosecond photoionization of coherently coupled electronic states *Phys. Rev.* A **72** 051401
[48] Weinkauf R, Schanen P, Yang D, Soukara S and Schlag E W 1995 Elementary processes in peptides: electron mobility and dissociation in peptide cations in the gas phase *J. Phys. Chem.* **99** 11255
[49] Weinkauf R, Schlag E W, Martinez T J and Levine R D 1997 Nonstationary electronic states and site-selective reactivity *J. Phys. Chem.* A **101** 7702
[50] Cederbaum L S and Zobeley J 1999 Ultrafast charge migration by electron correlation *Chem. Phys. Lett.* **307** 205
[51] Barth I and Manz J 2006 Periodic electron circulation induced by circularly polarized laser pulses: quantum model simulations for Mg porphyrin *Angew Chem. Int. Ed.* **45** 2962
[52] Mineo H, Yamaki M, Teranishi Y, Hayashi M, Lin S H and Fujimura Y 2012 Quantum switching of p-electron rotations in a nonplanar chiral molecule by using linearly polarized UV laser pulses *J. Am. Chem. Soc.* **134** 14279

[53] Kanno M, Kono H, Fujimura Y and Lin S H 2010 Nonadiabatic response model of laser-induced ultrafast π-electron rotations in chiral aromatic molecules *Phys. Rev. Lett.* **104** 108302
[54] Varela K, Hargreaves L R, Ralphs K, Khakoo M A, Winstead C, McKoy V, Rescigno T N and Orel A E 2015 Excitation of the 4 lowest electronic transitions in methanol by low-energy electrons *J. Phys. B: At. Mol. Opt. Phys.* **48** 115208
[55] Qi Y, Shu C C, Dong D, Petersen I R, Jacobs K and Gong S 2019 Fast quantum state transfer in hybrid quantum dot-metal nanoparticle systems by shaping ultrafast laser pulses *J. Phys. D: Appl. Phys.* **52** 425101
[56] Mignolet B, Levine R D and Remacle F 2014 Charge migration in the bifunctional PENNA cation induced and probed by ultrafast ionization: a dynamical study *J. Phys. B: At. Mol. Opt. Phys.* **47** 124011
[57] Despré V, Marciniak A, Loriot V, Galbraith M C E, Rouzée A, Vrakking M J J, Lépine F and Kuleff A I 2015 Attosecond hole migration in benzene molecules surviving nuclear motion *J. Phys. Chem. Lett.* **6** 426
[58] Despré V, Golubev N V and Kuleff A I 2018 Charge migration in propiolic acid: a full quantum dynamical study *Phys. Rev. Lett.* **121** 203002
[59] Shao H C and Starace A F 2016 Imaging population transfer in atoms with ultrafast electron pulses *Phys. Rev.* A **94** 030702
[60] Barth I, Manz J, Shigeta Y and Yagi K 2006 Unidirectional electronic ring current driven by a few cycle circularly polarized laser pulse: quantum model simulations for Mg-porphyrin *J. Am. Chem. Soc.* **128** 7043
[61] Yuan K J and Bandrauk A D 2016 Monitoring coherent electron wave packet excitation dynamics by two-color attosecond laser pulses *J. Chem. Phys.* **145** 194304
[62] Diestler D J, Hermann G and Manz J 2017 Charge migration in Eyring, Walter and Kimball's 1944 model of the electronically excited hydrogen-molecule ion *J. Phys. Chem. A.* **121** 5332
[63] Wörner H J *et al* 2017 Charge migration and charge transfer in molecular systems *Struct. Dyn.* **4** 061508
[64] Calegari F, Trabattoni A, Palacios A, Ayuso D, Castrovilli M C, Greenwood J B, Decleva P, Martín F and Nisoli M 2016 Charge migration induced by attosecond pulses in bio-relevant molecules *J. Phys. B: At. Mol. Opt. Phys.* **49** 142001
[65] Miller M R, Xia Y, Becker A and Jaron-Becker A 2016 Laser driven nonadiabatic electron dynamics in molecules *Optica* **3** 259
[66] Mineo H, Lin S H and Fujimura Y 2013 Coherent electron dynamics of (P)-2,2-biphenol induced by ultrashort linearly polarized UV pulses: angular momentum and ring current *J. Chem. Phys.* **138** 074304
[67] Hermann G, Liu C, Manz J, Paulus B, Pérez-Torres J F, Pohl V and Tremblay J C 2016 Multidirectional angular electronic flux during adiabatic attosecond charge migration in excited benzene *J. Phys. Chem. A.* **120** 5360
[68] Hermann G, Liu C, Manz J, Paulus B, Pohl V and Tremblay J C 2017 Attosecond angular flux of partial charges on the carbon atoms of benzene in non-aromatic excited state *Chem. Phys. Lett.* **683** 553
[69] Jia D, Manz J, Paulus B, Pohl V, Tremblay J C and Yang Y 2017 Quantum control of electronic fluxes during adiabatic attosecond charge migration in degenerate superposition states of benzene *Chem. Phys.* **482** 146
[70] Kraus P M *et al* 2015 Measurement and laser control of attosecond charge migration in ionized iodoacetylene *Science* **790** 350
[71] Yuan K J and Bandrauk A D 2017 Exploring coherent electron excitation and migration dynamics by electron diffraction with ultrashort x-ray pulses *Phys. Chem. Chem. Phys.* **19** 25846
[72] Yuan K J and Bandrauk A D 2018 Time-resolved photoelectron imaging of molecular coherent excitation and charge migration by ultrashort laser pulses *J. Phys. Chem. A.* **122** 2241
[73] Yuan K J and Bandrauk A D 2019 Ultrafast x-ray photoelectron imaging of attosecond electron dynamics in molecular coherent excitation *J. Phys. Chem. A.* **123** 1328
[74] He M, Li Y, Zhou Y, Li M, Cao W and Lu P 2018 Direct visualization of valence electron motion using strong-field photoelectron holography *Phys. Rev. Lett.* **120** 133204
[75] He M, Zhou Y, Tan J, Li Y, Li M and Lu P 2018 Imaging charge migration in the asymmetric molecule with the holographic interference in strong-field tunneling ionization *J. Phys. B: At. Mol. Opt. Phys.* **51** 245602
[76] Ibrahim H, Lefebvre C, Bandrauk A D, Staudte A and Légaré F 2018 H_2: the benchmark molecule for ultrafast science and technologies *J. Phys. B: At. Mol. Opt. Phys.* **51** 042002
[77] Stapelfeldt H and Seideman T 2003 Aligning molecules with strong laser pulses *Rev. Mod. Phys.* **75** 543
[78] Yuan K J, Lu H Z and Bandrauk A D 2011 Linear- and circular-polarization photoionization angular distributions in H_2 and H_2^+ by attosecond XUV laser pulses *Phys. Rev.* A **83** 043418
[79] Bandrauk A D and Shen H 1993 Exponential split operator methods for solving coupled time-dependent Schrödinger equations *J. Chem. Phys.* **99** 1185
[80] Bandrauk A D and Lu H Z 2013 Exponential propagators (integrators) for the time-dependent Schrödinger equation *J. Theor. Comput. Chem.* **12** 1340001
[81] Yuan K J, Lu H Z and Bandrauk A D 2009 Laser-induced electron diffraction in H_2 with linear and circular polarization ultrashort XUV laser pulses *Phys. Rev.* A **80** 061403
[82] Mulliken R S 1937 Low electronic states of simple heteropolar diatomic molecules: III. Hydrogen and univalent metal halides *Phys. Rev.* **51** 310
[83] Yuan K J and Bandrauk A D 2015 Molecular alignment dependent electron interference in attosecond ultraviolet photoionization *Struct. Dyn.* **2** 014101
[84] Pronin E A, Starace A F, Frolov M V and Manakov N L 2009 Perturbation theory analysis of attosecond photoionization *Phys. Rev.* A **80** 063403
[85] Young L *et al* 2018 Roadmap of ultrafast x-ray atomic and molecular physics *J. Phys. B: At. Mol. Opt. Phys.* **51** 032003
[86] Ueda K *et al* 2019 Roadmap on photonic, electronic and atomic collision physics: I. Light–matter interaction *J. Phys. B: At. Mol. Opt. Phys.* **52** 171001
[87] Schippers S *et al* 2019 Roadmap on photonic, electronic and atomic collision physics: II. Electron and antimatter interactions *J. Phys. B: At. Mol. Opt. Phys.* **52** 171002